Available online at www.sciencedirect.com

ScienceDirect

Geochimica et Cosmochimica Acta 164 (2015) 352–364

Geochimica et Cosmochimica Acta

www.elsevier.com/locate/gca

# Ediacaran sulfur cycle: Insights from sulfur isotope measurements ($\Delta^{33}S$ and $\delta^{34}S$) on paired sulfate–pyrite in the Huqf Supergroup of Oman

Nanping Wu [a,b,*], James Farquhar [a], David A. Fike [c]

[a] Department of Geology, University of Maryland, College Park, MD 20740, United States
[b] Department of Earth Sciences, University of New Hampshire, Durham, NH 03824, United States
[c] Department of Earth and Planetary Sciences, Washington University, St. Louis, MO 63130, United States

Received 20 June 2014; accepted in revised form 19 May 2015; Available online 27 May 2015

**Abstract**

The Ediacaran Period (635–541 Ma) was a time of dramatic environmental and ecological change. Sulfur isotopic records preserved in marine strata provide insights into these changes. Previous work using $\delta^{34}S$ in pyrite and carbonate-associated sulfate in the Ediacaran-aged Huqf Supergroup (Sultanate of Oman) suggested increases in marine sulfate concentrations, changing microbial pathways and redox conditions, and a long-term increase in $\delta^{34}S$ of sulfate delivery to the ocean. However, $\delta^{34}S$-based analyses on their own were insufficient to uniquely reconstruct these environmental and ecological changes. Here we present new paired $\delta^{34}S$ and $\Delta^{33}S$ data from carbonate-associated sulfate and pyrite in these strata. The results allow us to provide three new constraints on Ediacaran sulfur cycling. First, a notable increase $\Delta^{34}S_{CAS\text{-}PY}$, previously attributed to possible disproportionation, in upper Buah strata is associated with $\Delta^{33}S$-evidence for an increase in sulfide reoxidation, indicating a transition to more oxidizing conditions, possibly associated with the onset of bioturbation. Secondly, $\Delta^{33}S$ data indicate that a large positive shift in both sulfate and pyrite $\delta^{34}S$ in Ara Group strata is mostly likely due to an increase in delivery of $^{34}S$-enriched sulfate to the basin. Finally paired $\delta^{34}S$–$\Delta^{33}S$ data constrain possible changes in seawater sulfate concentrations, suggesting an increase in sulfate supply related to enhanced evaporite weathering, consistent with geological and geochemical observations that imply high $[SO_4]$ (~17 mM) during deposition of the Ara Group.


## 1. INTRODUCTION

Earth's surface environments, its biology, and its ecology underwent a series of dramatic changes during the transition from the late Ediacaran to the early Cambrian periods. The Ediacaran biota, large architecturally complex organisms, disappeared and were succeeded by the radiation of metazoan phyla of the Cambrian Explosion (Narbonne, 2005; Laflamme et al., 2013). The biological innovations brought by these organisms had a significant impact on the global carbon cycle, the history of which is recorded by carbonate minerals and organic matter in sedimentary rocks at this time (Bartley and Kah, 2004; Maloof et al., 2010). The evolution of the sulfur cycle at this time provides information about linkages between biological evolution, ecosystem construction and the Earth's environmental change (Fike et al., 2006; McFadden et al., 2008; Johnston et al., 2012, 2013; Xiao et al., 2012; Li et al., 2013; Loyd et al., 2013).

A number of scientific questions have been raised by studies of the Ediacaran sulfur cycle that are linked to isotopic measurements of sulfide and sulfate. These include

* Corresponding author at: Department of Earth Sciences, University of New Hampshire, Durham, NH 03824, United States. Tel.: +1 603 312 7655.
*E-mail address:* wunanping@gmail.com (N. Wu).

http://dx.doi.org/10.1016/j.gca.2015.05.031
0016-7037/

questions about the levels of sulfate in oceans basins, the evolution of sulfide oxidation in the sediments, the role of bioturbation as an agent of sulfur cycling, and whether the isotopic records of sulfide and sulfate from different basins preserve signatures of the global ocean, or instead, regional signals. Evaluating the connections between sulfur isotope fractionation, sulfate concentrations, and sulfide reoxidation is considered a key step for better understanding the evolution of the Ediacaran sulfur cycle and its relationship to the carbon cycle.

The late Neoproterozoic deep oceans, immediately before and extending into the Ediacaran, became progressively more oxygenated (Fike et al., 2006; Canfield et al., 2007, 2008; Dahl et al., 2010) and may have triggered the evolution of a number of groups of benthic eukaryotic organisms (Canfield et al., 2007; McFadden et al., 2008). Some of these organisms would have bioturbated sediments, creating conditions that may have enhanced oxidation of sedimentary sulfide and played an important role regulating oceanic sulfate levels; such changes may also have had a significant impact on the sulfur isotopic compositions of oceanic sulfate and sedimentary pyrite formed at this time (Canfield and Farquhar, 2009). Other factors that influenced oceanic sulfate concentrations and its sulfur isotopic compositions in the Ediacaran include possible changes in sulfate input to the oceans associated with enhanced evaporite weathering over short time-scales (Halevy et al., 2012; Wortmann and Adina Paytan, 2012) or longer-term evolution of $\delta^{34}S$ from continental weathering (Canfield, 2004; Fike and Grotzinger, 2008). Such changes in sulfate concentration could leave an isotopic signature of a reservoir effect on seawater sulfate. Such changes may have also influenced the fraction of sulfur buried as pyrite, and in turn the isotopic composition of the sedimentary sulfide pool (Wortmann and Chernyavsky, 2007; Wortmann and Adina Paytan, 2012).

Constraints on oceanic sulfate concentrations in the Ediacaran come from fluid inclusion studies in rocks from the Ara Group of the Huqf Supergroup in Oman (Horita et al., 2002; Lowenstein et al., 2003), from sulfur isotope evidence of the Doushantuo Formation in the Nanhua Basin, South China (McFadden et al., 2008; Li et al., 2010a), and from modeling results based on the rate of change in sulfate–sulfur isotopic compositions within carbonate strata of Sonora, Mexico and Death Valley, California (Loyd et al., 2012). These three different types of studies have yielded different interpretations. Fluid inclusion evidence points to high concentrations of oceanic sulfate (~17 mM). Sulfur isotopic variability suggests much lower sulfate levels (~0.2 mM). Finally, simulations suggest sustained low sulfate conditions (~2.0 mM or lower).

Here, we present measurements of $\Delta^{33}S$ (and $\delta^{34}S$) of paired carbonate-associated sulfate (CAS) and sedimentary pyrite for samples previously studied from the Huqf Supergroup in the Oman basin (Fike et al., 2006; Fike and Grotzinger, 2008). This prior work suggested progressive change in the Ediacaran sulfur cycle, but was unable to distinguish between a cause related to a geo-biological response to changing conditions such as higher sulfate concentrations or a cause tied to influx of $^{34}S$-enriched sulfate to the oceans. First, an increase in $\Delta^{34}S_{CAS\text{-}PY}$ from ~10‰ to 30‰ from ~635 Ma to ~580 Ma suggested an increase in sulfate concentrations (Fike et al., 2006). Secondly, a further increase in $\Delta^{34}S_{CAS\text{-}PY}$ to 53‰ around 548 Ma was interpreted as possible evidence of the oxidative sulfur cycle and sulfur disproportionation (Fike et al., 2006). However, interpretations of $\Delta^{34}S_{CAS\text{-}PY}$ are non-unique and many other factors (e.g., sulfate concentration, sulfate reduction rate, organic carbon availability) may have also been a factor in these trends. Finally, a substantial increase in $\delta^{34}S$ from both sulfate and pyrite was observed moving into strata of the Ara Group (~547–540 Ma) (Fike and Grotzinger, 2008). Mass balance arguments suggested this was the result of an increase in pyrite burial against a backdrop of elevated $\delta^{34}S$ delivery to the oceans (Fike and Grotzinger, 2008), but $\delta^{34}S$ data alone were insufficient to estimate the relative impact of these two contributions.

Here we present new paired $\delta^{34}S$ and $\Delta^{33}S$ data from carbonate-associated sulfate and pyrite in these strata that allow us to provide new constraints on the operation of the Ediacaran sulfur cycle. The use of $\Delta^{33}S$ in addition to $\delta^{34}S$ to evaluate oceanic sulfate is a relatively recent innovation in sulfur cycle studies (c.f., Johnston et al., 2005, 2007, 2008a,b; Ono et al., 2006; Wu et al., 2010) and has the potential to provide additional ways to constrain the role of different sulfur metabolisms as well as to constrain sulfur fluxes through geologic time (Li et al., 2010b; Leavitt et al., 2013).

The measurements described for the Huqf Supergroup are used to gain new insights into the evolution of the Ediacaran marine sulfur cycle and the factors that influence the concentrations of seawater sulfate at this time. We evaluate hypotheses about changing oceanic sulfate concentrations and argue that connections between sulfur isotope fractionations, sulfate concentrations, and sulfide reoxidation revealed by the rare sulfur isotopes are generally consistent with existing models, with a few subtle differences. Specifically, it appears that the sulfur in the Oman basin at the end of the Ediacaran during the deposition of the Ara Group was fed by a $^{34}S$-enriched sulfate source. We propose that such a source may originate either as a result of enhanced evaporite weathering on a global scale, or as a result of a restriction-related process with the oceanic sulfate pool as the source of basin sulfate.

## 2. GEOLOGICAL CONTEXT

Studies of the Huqf Supergroup of Oman have informed understanding of the evolution of the Ediacaran sulfur cycle by providing evidence for high oceanic sulfate levels Ediacaran (15.5–25.0 mM), as estimated from halite fluid inclusions within evaporites of the Ara Group (Lowenstein et al., 2003; Brennan et al., 2004). The Huqf Supergroup is a thick sequence of strata consisting of the Abu Mahara, Nafun and Ara groups, with several recognized unconformities in the succession (Mattes and Conway-Morris, 1990; McCarron, 2000). The oldest part of the Huqf Supergroup, the Abu Mahara Group, overlies ~800 Ma crystalline basement and contains glacial deposits

of Marinoan age (~635 Ma, Bowring et al., 2007). The Nafun Group overlies the Abu Mahara Group and was deposited during the Ediacaran (ca. 635–547 Ma; Bowring et al., 2007). The Nafun Group was deposited in a shallow marine environment and outcrops can be traced laterally over a distance of several hundred kilometers (Mattes and Conway-Morris, 1990; McCarron, 2000; Grotzinger et al., 2002; Le Guerroue et al., 2006). The strata of the Nafun Group consist of two clastic-to-carbonate shallowing-upward cycles: the older cycle is comprised of the Masirah Bay and Khufai formations; the younger cycle, the Shuram and Buah formations.

A negative excursion in $\delta^{13}C_{carb,}$ reaching a minimum of about −12‰, is found in the Shuram Formation, Oman (Burns and Matter, 1993), as well as in several other Ediacaran successions, including the Johnnie Formation, Western United States (Kaufman et al., 2007); the Doushantuo Formation, South China (McFadden et al., 2008); and the Wonoka Formation, Australia (Calver, 2000). This extreme shift in $\delta^{13}C_{carb}$, known as the Shuram excursion, is thought to be a global event which is possibly attributable to oxidation of organic matter in the deep ocean (Fike et al., 2006; Grotzinger et al., 2011). The Shuram excursion begins at the transition between the Khufai and basal Shuram formations and extends through the mid-Buah Formation. The onset of the Shuram excursion is thought to post-date the interval of Gaskiers glaciation (~580 Ma) (McCarron, 2000; Bowring et al., 2002, 2007).

The Ara Group overlies the Nafun Group and was deposited between ~547 Ma and 540 Ma (Bowring et al., 2007) in a subsiding, fault-bounded basin (South Oman Salt Basin, SOSB) (Mattes and Conway-Morris, 1990; Schröder et al., 2003, 2005). In the basin, the Ara Group consists of a series of seven carbonate shallowing upwards cycles (A0–A6) with evaporites discontinuously present in the upper six, indicating recurring basin restriction. In the eastern flank of the SOSB, the Ara Group does not preserve evaporites and these carbonates may have been deposited in connection with the open ocean (Amthor et al., 2003; Fike, 2007; Fike and Grotzinger, 2008). The thickness of the Ara Group (A0–A6) is approximately 200–300 m in the eastern flank of the SOSB, but is more variable and can be well over 1 km in the SOSB interior.

The Ara Group in the eastern flank shares an unconformable contact with the underlying Buah Formation. The age of the upper Buah Formation is believed to be ~548 Ma based on $\delta^{13}C_{carb}$ correlation to Namibia (Grotzinger et al., 1995). Another constraint for the basal Ara Group (A0 carbonate unit) is provided by an ash horizon that has been determined to be 546.72 ± 0.21 Ma (Bowring et al., 2007). These ages suggest the unconformity at the Buah-Ara boundary is less than 1 Myr in duration. Within the Ara Group, A4 carbonates can be readily correlated between the basin (SOSB) and the eastern flank based on the presence of a bedded ash horizon, dated to 541 Ma (Bowring et al., 2007) and a negative carbon isotope excursion (~7‰), which marks the Ediacaran–Cambrian boundary (Amthor et al., 2003).

## 3. RESULTS

Sulfur isotope data for carbonate-associated sulfate and pyrite are reported in appendix tables (Tables A1 and A2). Fig. 1 presents the carbon and sulfur isotope data along the stratigraphic column in the Huqf Supergroup, which is normalized to the MQR-1 well depths. Information about samples, and also about the analytical methods used to obtain the data herein, are described in detail in the Supplementary material.

Fig. 1 presents the sulfur isotope data ($\delta^{34}S$ and $\Delta^{33}S$) using the $SF_6$ method and also includes the isotopic data ($\delta^{34}S$) reported in Fike et al. (2006) and Fike and Grotzinger (2008) collected using an on-line combustion technique coupled with isotope ratio monitoring of $SO_2$. A cross plot of $SF_6$ measurements against previous $SO_2$-based analyses at the stable isotope lab of Indiana University yields a relationship of $\delta^{34}S_{SF6} = 1.013(\pm 0.007; 1\sigma) \times \delta^{34}S_{SO2}$-0.234(±0.171; 1σ), where the value of the regression correlation coefficient is 0.994. Any differences between these two methods are thought to be due to scale compression and memory effects associated with the $SO_2$-based method (Rees, 1978). The comparison of the results based on these two methods shows that the general match is good for analyses made in the present study and those of Fike et al. (2006) and Fike and Grotzinger (2008) on the same extracts (CAS samples in the form of barite powder and chromium reducible sulfur was in form of silver sulfide). The following data analysis and interpretation is based on the sulfur isotope data measured by $SF_6$ method.

At the Buah–Ara boundary, a positive shift (~15‰) in the $\delta^{34}S$ of sulfate is observed, which has been called the Ara anomaly (Fike and Grotzinger, 2008). $\delta^{34}S_{CAS}$ remains constant (~40‰) throughout the Ara Formation. There is also a positive shift (up to ~30‰) in $\delta^{34}S_{PY}$ at the Buah–Ara boundary, and $\delta^{34}S_{PY}$ remains positive and relatively constant (~10‰) throughout the Ara Formation.

The stratigraphic profiles for $\delta^{34}S$ of pyrite and CAS diverge throughout the Masirah Bay Formation and Buah Formation, indicating an increase in fractionation. These profiles then parallel each other in the Ara Group, indicating constancy in the magnitude of fractionation. Specifically, the sulfur isotope fractionations between sulfate and pyrite ($\Delta^{34}S_{CAS\text{-}PY}$) increases from a smaller value of approximately 10‰ in the Masirah Bay Formation to approximately 47‰ in the middle Shuram. Following this, $\Delta^{34}S_{CAS\text{-}PY}$ decreases to 26‰ in the uppermost Shuram, before rising to reach a maximum value of approximately 53‰ in the upper Buah. A drop in the magnitude of $\Delta^{34}S_{CAS\text{-}PY}$ occurs at the boundary of Buah–Ara to reach a fractionation of approximately 30‰.

Stratigraphic profiles for $\Delta^{33}S_{PY}$ and $\Delta^{33}S_{CAS}$ covary throughout the Huqf Supergroup. $\Delta^{33}S_{CAS}$ gradually rises from −0.053‰ to 0.048‰ in the Masirah Bay Formation and lower Khufai Fm., and $\Delta^{33}S_{CAS}$ then falls to −0.009‰ followed by an increase to 0.066‰ in the uppermost Khufai Fm. $\Delta^{33}S_{CAS}$ then falls to −0.007‰ and rises to 0.026‰ just prior to the boundary of Khufai–Shuram

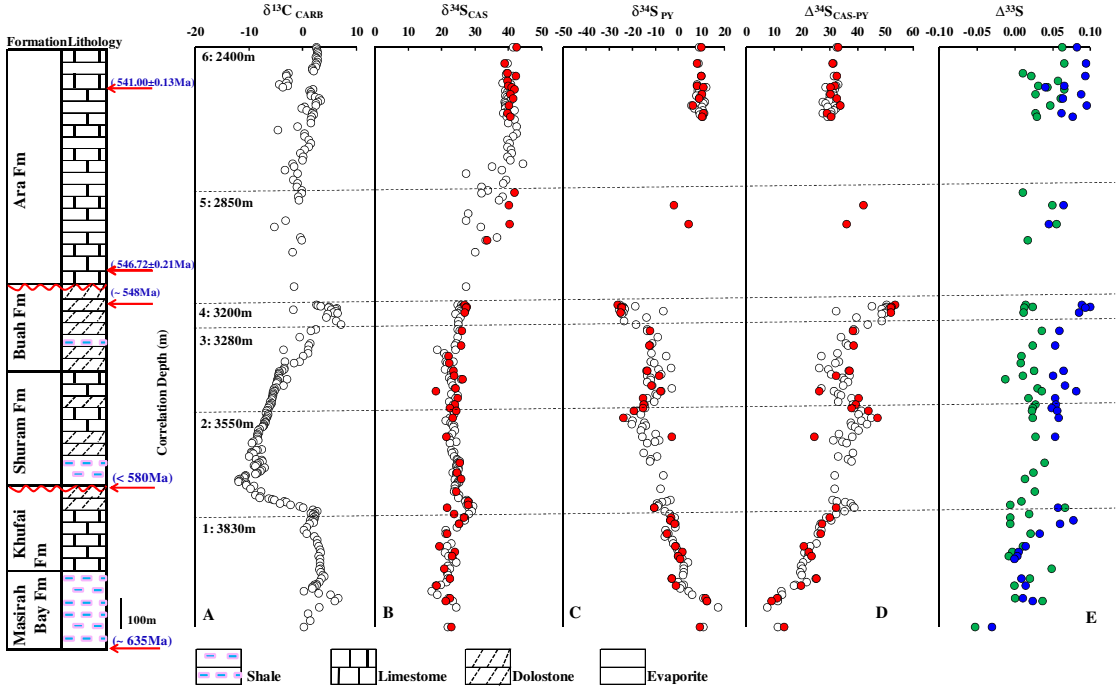


Fig. 1. Composite $\delta^{13}C_{carb}$, $\delta^{34}S$ and $\Delta^{33}S$ profiles of carbonate, sulfate and pyrite along the normalized strata depth. Carbon isotope data and $SO_2$-based analyses of sulfur isotope data ($\delta^{34}S$, open white circles in panels A, B and C) are reported in studies of Fike et al. (2006) and Fike and Grotzinger (2008). The new $SF_6$-based analyses of sulfur isotope data are also presented (red circles in panels B and C). The panel D is the sulfur isotope fractionation ($\Delta^{34}S_{CAS\text{-}PY}$) between sulfate and pyrite. The panel E is the $\Delta^{33}S$ profile for sulfate (green dots) and pyrite (blue dots), respectively. The error bar (0.16‰, 2$\sigma$) in $\delta^{34}S$ profile is smaller than the data symbol, and the error bar (2$\sigma$) in $\Delta^{33}S$ profile is 0.012‰. Ages constraints in the composite strata column are from correlation to other sections including U–Pb dating age on ash beds. Detailed description of sulfur isotope data is seen in text. Strata are subdivided into 6 intervals on the basis of geological observations (lithostratigraphic transitions and unconformities observed in the strata) and coherent relationships for the sulfur isotopic compositions of sulfate and pyrite. See more in text and also refer to Fig. 2. (For interpretation of the references to color in this figure legend, the reader is referred to the web version of this article.)

formations. $\Delta^{33}S_{CAS}$ then oscillates around a mean of 0.020‰ for most of the Shuram and Buah Formations. There is a slightly positive shift in $\Delta^{33}S_{CAS}$ (up to 0.020‰) at the boundary of Buah–Ara Formations. $\Delta^{33}S_{PY}$ shows similar variations and oscillations, tracking the $\Delta^{33}S_{CAS}$ record. Values of $\Delta^{33}S_{PY}$ are generally higher than those for $\Delta^{33}S_{CAS}$ (average offset of 0.014‰, refer to Tables A1 and A2). The $\Delta^{33}S_{PY}$ reaches maximum of 0.099‰ in the uppermost Buah. $\Delta^{33}S$ of pyrite and sulfate similarly show more scattered values with averages of 0.072‰ and 0.039‰, respectively, in the Ara Group.

## 4. DISCUSSION

### 4.1. Data evaluation

The carbonate samples with minimal diagenetic alternations were selected for carbonate associated sulfate extraction. The relationship between $\delta^{34}S$ and indicators of diagenesis ($\delta^{18}O_{carb}$, Mn/Sr, $\delta^{13}C_{carb}$, and the concentration of carbonate-associated sulfate) has been examined and no correlations were found (Fike et al., 2006), so it is believed depositional $\delta^{34}S$ are preserved. But other issues remains, for instance, non CAS sulfate contamination and its effect on isotopic compositions of CAS. The CAS samples studied here were rinsed and soaked in deionized water for 24 h to remove non CAS sulfate, which were derived from post-depositional pyrite oxidation and reduced sulfur oxidation in the lab extraction procedure (Wotte et al., 2012). Although it is difficult to quantitatively evaluate how non-sulfate influenced the final isotopic analysis due to paucity of data (e.g., the concentration of reduced sulfur in samples and oxidized rate of reduced sulfur in lab environments), the corrected $\delta^{34}S$ values of oceanic sulfate, if possible, would be much higher if measured $\delta^{34}S$ values of CAS are mixture with the sulfate derived from the oxidized pyrite, as seen from the depth profile of $\delta^{34}S$ of CAS that is generally higher than that of pyrite. Further, the $\delta^{34}S$ of CAS in carbonate units of the Ara Formation is consistent with the higher $\delta^{34}S$ of anhydrites that are interlayed by carbonate units, if the small sulfur isotope fractionation (~2‰, Raab and Spiro, 1991) associated with the gypsum/anhydrite formation is corrected (Schröder et al., 2004; Fike and Grotzinger, 2008), indicating the carbonate/evaporite units were deposited in marine environments that connected with the global ocean, and the $\delta^{34}S$

of CAS reflect primary signals. Thus we believe that the analytical procedure is not likely to affect the data analysis and interpretation.

### 4.2. Grouping of data

In order to capture the first-order features of the sulfur isotopic records and to simplify the interpretation of the isotopic records for sulfate and pyrite, $\delta^{34}S$ and $\Delta^{33}S$ provided in this study have been subdivided into six intervals on the basis of geological observations (lithostratigraphic transitions and unconformities observed in the strata) and coherent relationships for the sulfur isotopic compositions of sulfate and pyrite. These intervals correspond to (from oldest to youngest): (1) pre-Shuram excursion strata [Masirah Bay and Khufai formations]; (2) peak Shuram excursion strata [top Khufai – lower Shuram formations]; (3) recovery from the Shuram excursion [upper Shuram Formation and lower Buah Formation]; (4) uppermost Buah Formation; (5) basal Ara strata; (6) middle and upper Ara strata. These averages are summarized in Tables 1 and 2 and in Fig. 2.

The averages for $\delta^{34}S$ and $\Delta^{33}S$ values in sulfate progress from low values to high values moving up section from interval 1 to 6. The averages for $\delta^{34}S$ values of pyrite show a decrease between intervals 1–4, and then shift to positive values moving up into intervals 5 and 6. The averages for $\Delta^{33}S$ of pyrite show a general increase between the depths of intervals 1–4, and reach a maximum at the top of interval 4. Averages for $\Delta^{33}S$ of pyrite then shows a slight fall, but values remain high up section.

### 4.3. First order interpretation of sulfur isotopes

The magnitude of sulfur isotope fractionations ($\Delta^{34}S_{CAS\text{-}PY}$) between seawater sulfate and sedimentary pyrite reflects the combined effects of sulfur isotope fractionations by microbial sulfate reducers and pathways associated with sulfide oxidation and sulfur disproportionation, as well as other environmental factors such as temperature, sulfate concentration, sulfate supply and the type and abundance of reactive organic carbon. The use of sulfur by these organisms may also respond to changes in these environmental factors, with changes in sulfate reduction rate and sulfur isotope fractionation that may reflect different oceanic settings such as sulfate limitation (Canfield, 2001; Detmers et al., 2001; Habicht et al., 2002; Wing and Halevy, 2014).

Studies have shown that the magnitude of the biological fractionation associated with microbial sulfate reduction is related to the sulfate concentrations in the growth medium (Habicht et al., 2002; Bradley et al., in revision) and cell specific sulfate reduction rate (Leavitt et al., 2013; Wing and Halevy, 2014). Sulfate reducers have shown a capability of producing very large isotopic fractionation when sulfate concentrations are above 0.2 mM (Canfield, 2001; Habicht et al., 2002; Canfield et al., 2010). Studies also have shown that sulfate reducers metabolizing sulfate in settings where the sulfate concentrations are low (<0.2 mM), express much smaller sulfur isotope fractionations (Habicht et al., 2002; Gomes and Hurtgen, 2013). This arises because at low sulfate concentrations the uptake of sulfate in the sequence of metabolic steps associated with sulfate reduction is the rate limiting step, so that large fractionations are not expressed in the final metabolic product. However, more recent studies show the relationship between isotope fractionation associated with microbial sulfate reduction and environmental sulfate concentrations is more complicated. A recent study shows large fractionations at micromolar sulfate levels (Crowe et al., 2014) and the theoretical study by Wing and Halevy (2014) also suggests that large fractionations are possibly expressed and preserved in sedimentary or geological records at low sulfate concentrations, where slow respiration rates of microbial sulfate reducers are sustained.

Fike et al. (2006) and Fike and Grotzinger (2008) have interpreted the smaller fractionations, $\Delta^{34}S_{CAS\text{-}PY}$ (Figs. 1 and 2), in the lower parts of the Huqf Supergroup (stage 1) in terms of sulfate limitation – possibly as low as 0.2 mM (consistent with inferences from Hurtgen et al. (2006) for low sulfate concentrations in the immediate aftermath of the Marinoan glaciation), and suggested that the larger fractionations overlying strata (stages 2 and 3) reflect rising sulfate concentrations. Values of $\Delta^{34}S_{SW\text{-}PY}$ as high as ~53‰ seen in the interval between 3224 and 3200 m (stage 4), are very large and it has been suggested that they reflect an added role of sulfur disproportionation in a more complex model of sulfur cycling (Fike et al., 2006). Recent studies have suggested that it is also possible that they represent a single step of microbial sulfate reduction (see Wortmann et al., 2001; Rudnicki et al., 2001; Brunner and Bernasconi, 2005; Canfield et al., 2010; Sim et al., 2011). The $\delta^{34}S$ values of pyrite for stage 4 are the lowest values seen in the succession. Likewise the $\Delta^{33}S$ values of pyrite for stage 4 are the highest and point to a change in sulfur isotope fractionation, possibly a change in the way sulfur is cycled. The $\Delta^{33}S_{PY}$ data do not

Table 1
Averages of $\delta^{34}S$ and $\Delta^{33}S$ of CAS for binned strata.

| Stage | Strata unit | $\delta^{34}S$ (‰, 2$\sigma$) | $\Delta^{33}S$ (‰, 2$\sigma$) |
|---|---|---|---|
| 6 | Ara Fm | 40.5 ± 0.6 | 0.042 ± 0.010 |
| 5 | Ara Fm | 38.9 ± 3.7 | 0.033 ± 0.022 |
| 4 | Buah Fm | 26.8 ± 0.5 | 0.019 ± 0.009 |
| 3 | Shuram Fm, Buah Fm | 23.3 ± 1.1 | 0.018 ± 0.007 |
| 2 | Khufai Fm, Shuram Fm | 24.9 ± 1.6 | 0.019 ± 0.010 |
| 1 | Khufai Fm, Masirah Fm | 22.2 ± 1.2 | 0.010 ± 0.015 |

Table 2
Averages of $\delta^{34}S$ and $\Delta^{33}S$ of pyrite for binned strata.

| Stage | Strata unit | $\delta^{34}S$ (‰, 2$\sigma$) | $\Delta^{33}S$ (‰, 2$\sigma$) |
|---|---|---|---|
| 6 | Ara Fm | 9.2 ± 0.9 | 0.075 ± 0.011 |
| 5 | Ara Fm | 1.1 ± 6.4 | 0.054 ± 0.019 |
| 4 | Buah Fm | −25.3 ± 0.9 | 0.091 ± 0.006 |
| 3 | Shuram Fm, Buah Fm | −13.3 ± 2.2 | 0.058 ± 0.006 |
| 2 | Khufai Fm, Shuram Fm | −13.5 ± 21.0 | 0.055 ± 0.004 |
| 1 | Khufai Fm, Masirah Fm | 0.3 ± 3.4 | 0.032 ± 0.028 |

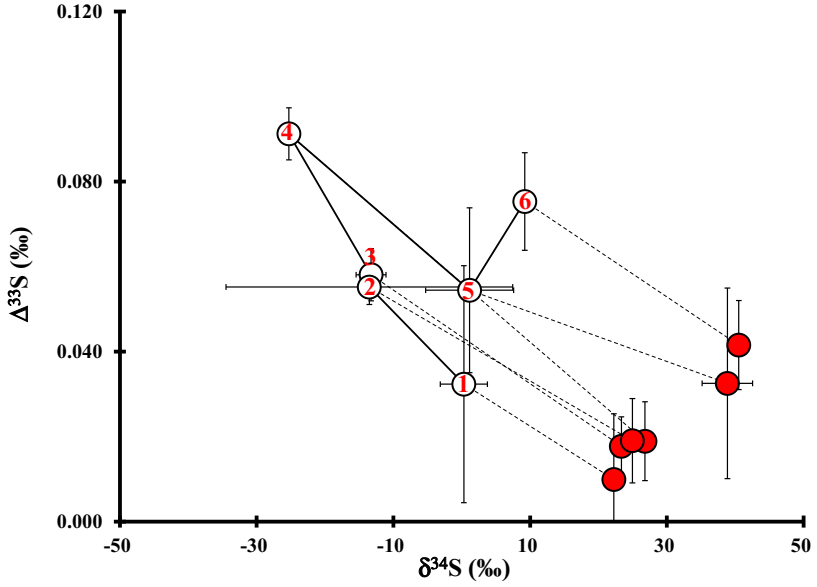


Fig. 2. Plot shows averages for different stratigraphic intervals that extended from lower in the sequence (stage 1) to the upper sequence (stage 6). Bars on points are standard deviations ($2\sigma$) of averages for the different stratigraphic horizons. The gray dashed lines link the compositions of corresponding sulfate and pyrite for each binned stratigraphic interval. This figure illustrates the evolution of oceanic sulfate (red dots) from $\delta^{34}S$ values near 22‰ and $\Delta^{33}S$ values near 0.010‰ to a set of higher values. This plot tracks a clockwise evolution of pyrite sulfur (white circles) moving up section. (For interpretation of the references to color in this figure legend, the reader is referred to the web version of this article.)

explicitly require additional microbial processing by sulfur disproportionation, however, nor do they preclude it. Mass balance considerations may also imply that the fraction of pyrite burial at this stage was lower than in other times represented by the stratigraphy. This is consistent with the oxidized nature of these sediments (high iron-oxide content, low TOC, low pyrite abundance; Fike et al. (2006)).

The sulfur isotope fractionation ($\Delta^{34}S_{CAS\text{-}PY}$) in the overlying Ara Group (stages 5 and 6) first drops to ~40‰ and then ~30‰, and has been interpreted to reflect a less important role for sulfur disproportionation (Fike and Grotzinger, 2008). The positive shift for $\delta^{34}S$ of both the pyrite and the carbonate-associated sulfate from stage 4 to stage 5, and then to even higher $\delta^{34}S$ and $\Delta^{33}S$ values for both sulfate and pyrite at stage 6 may support a Rayleigh distillation-like model of sulfur cycling with an enhanced pyrite burial sink, or alternatively, this may indicate a shift in composition for influx sulfate to very positive $\delta^{34}S$ or both (Canfield, 2004; Fike and Grotzinger, 2008).

### 4.4. Evaluating sulfur isotopes using steady-state models

Many of these first order interpretations of the Huqf Supergroup have been developed using a perspective of steady-state mass balance models that assume: (1) there are three major sulfur pools (seawater sulfate, sulfate evaporite minerals, and pyrite), (2) other sulfur pools are negligible, (3) the sulfur cycle is closed in terms of exchange of sulfur between mantle and the Earth surface, and (4) the sulfur isotope compositions of influx sulfate to the oceans may change with time. From a mathematical viewpoint, modeling of oceanic sulfate at steady state yields properties (e.g., sulfur isotopic compositions) that do not change with time.

We justify use of a steady state model to constrain the sulfur cycle during deposition of Huqf Supergroup on the basis of two lines of reasoning. The first is made by comparing sampling density with estimates made on residence time for oceanic sulfate at this time (~1 Myr). The second is made through examination of the sulfur cycle in continuous records that are interpreted to reflect transient steady – state conditions. The assumption of the sulfur cycle at steady state conditions does not imply oceanic sulfate levels were constant over significant intervals of geologic time, but instead it implies that the response time of oceanic sulfate–sulfur isotopes due to the perturbation of the sulfur cycle matches the residence time of oceanic sulfate–sulfur.

Using an age model that is based on the assumed age of the basal diamictite and radiometric constraints within the Huqf succession (Bowring et al., 2007), the temporal resolution of samples analyzed here is on the order of every one to a few million years. This sample resolution is comparable to the turnover times estimated for low sulfate (<5 mM) oceans by Kah et al. (2004) and Canfield and Farquhar (2009). Canfield and Farquhar (2009) arrive at similar order of magnitude residence times using a relationship relating the sulfate sink to evaporite formation, reoxidation and sulfate reduction rates, which depend on the reactive organic carbon flux and penetration of sulfate into the sediments. The way to deal with the sulfur cycle under steady state conditions is informative and is the first step to quantitatively understand the evolution of the sulfur cycle over geologic time.

Non-steady state processes (e.g., changes in sulfate concentrations) may contribute to high order oscillations in the studied isotope signatures. A series of transient steady states can also be explored for evaluating the sulfur isotope data described herein in terms of the fraction of pyrite burial ($f_{py}$) and the fractionation between sulfate and buried pyrite ($\Delta^{34}S_{SW\text{-}PY}$) to provide insights about the evolution of the sulfur cycle at this time.

The differences in $\Delta^{33}S$–$\delta^{34}S$ space for these different stages (Tables 1 and 2, Fig. 2) suggest the sulfur cycle in the Oman basin evolved through a series of different states. The $\delta^{34}S_{PY}$ and $\Delta^{33}S_{PY}$ of stages 1, 2, and 3 are consistent with the possibility of a change in fractionation between sulfate and pyrite resulting from a change in sulfate concentrations (But the isotope data of pyrite may reflect sulfate reducers responded to other environmental changes, c,f., Canfield, 2001; Detmers et al., 2001; Habicht et al., 2002; Wing and Halevy, 2014). The relatively stable but slightly increasing $\delta^{34}S$ and $\Delta^{33}S$ of sulfate through these three stages may also reflect a combination of effects related to increasing sulfate levels and increasing sulfate exchange between seawater and sediment pore waters.

To evaluate this possibility, we use a model that includes both $\Delta^{33}S$ and $\delta^{34}S$ that is similar to other models presented previously (e.g., Johnston et al., 2005; Ono et al., 2006). The model used here includes additional steps that relate to sulfide oxidation and the exchange of sulfate between seawater and pore water sulfate pools such as in Zerkle et al. (2009). Parameters that are explored in this model include: (1) the fraction of pyrite burial ($f_{py}$), (2) the fraction of sulfide oxidation ($f_{reox}$), and (3) the fraction of sulfate exchange between seawater and pore-water ($f_{ex}$). Model results are compared with the isotopic data from the Huqf Supergroup in order to evaluate whether the model can be used to reproduce the results, and whether assumptions and the components in the model are valid. The details of the sulfur cycle model are discussed in the Supplementary materials.

The $f_{py}$ values can be estimated on the basis of $\Delta^{33}S$ and $\delta^{34}S$ of carbonate-associated sulfate. The $f_{py}$ values can be also derived using the common steady state equation based on paired $\delta^{34}S$ of sulfate and pyrite alone[1]. Both approaches require assumed $\delta^{34}S_{in}$ values of influx sulfur to the oceans, which is unknown, possibly variable, and potentially very positive at this period in Earth history (Canfield, 2004; Fike and Grotzinger, 2008). For instance, the $f_{py}$ values derived from multiple sulfur isotopes are 0.3–0.4 for stage 2 to stage 4 (Fig. 3) and are consistent with those values using the common steady state equation based on $\delta^{34}S$ alone, with an assumed $\delta^{34}S_{in}$ of ~10‰ (see Fig. 4). However, a minimum value of $\delta^{34}S_{in}$ ~25‰ is needed to result in similar $f_{py}$ values for stage 5 to stage 6 (see Fig. 4). The two different approaches can be reconciled if $\delta^{34}S_{in}$ increases across the transition to the Ara in this manner. [A similarly enriched $\delta^{34}S_{in}$ (~20‰) would be needed to produce consistent interpretations from paired $\delta^{34}S$ and $\delta^{34}S$–$\Delta^{33}S$ approaches for stage 1.] This approach using $\Delta^{33}S$–$\delta^{34}S$ of carbonate-associated sulfate provides a way to constrain the changes in $\delta^{34}S_{in}$ over geologic time afforded by isotope mass balance. On the other hand, the divergent estimates of $f_{py}$ using paired $\delta^{34}S$ or $\delta^{34}S$–$\Delta^{33}S$ in stage 1 and stages 5–6 could also indicate that the $\delta^{34}S$ and $\Delta^{33}S$ values in the basin may not be representative of the global averages of oxidized or reduced sulfur sinks at this time. This may imply that a local, rather than a global process is recorded by the carbonate-associated sulfate and/or pyrite in these intervals.

The shift in the sulfur isotopic composition of CAS to the sulfur isotopic compositions seen in stages 5 and 6 (Fig. 4) require more than a simple change in the fraction of pyrite burial and imply a change in the isotopic composition of the sulfate supply to the basin. The composition that is required (Fig. 4), suggests either an oceanic source or a significant change in the composition of influx sulfate such as that resulting from significant enhancements in evaporate weathering. We explore below the implications of each of these possibilities with model calculations.

#### 4.4.1. Model 1: Oceanic sulfate source to the Oman basin

Figs. 4 and 5 illustrates two possible scenarios that relate the isotopic compositions of sulfate in stages 5 and 6 to those seen in stages 1–4. Fig. 4 presents a steady-state analysis that assumes a $^{34}S/^{32}S$ fractionation associated with pyrite burial of ~25 ± 5‰ for the time interval of 580–545 Ma, which is inferred to be a reasonable estimate of the long-term average fractionation for successions of this age by Wu et al. (2010). The composition of the source sulfate to the system (global ocean or basin) should lie at a position on a mixing line that is determined by the fraction of pyrite buried ($f_{py}$).

In the first model, we explore the possibility that the sulfate source to the Oman basin for stages 5–6 is seawater sulfate from the open ocean. The possible range of compositions for the influx sulfate implied for stages 5–6 includes the compositions of inferred oceanic sulfate during stages 1–4. An origin that may require fewer changes to the sulfur cycle may therefore be a global oceanic sulfate pool that feeds a restricted basin during stages 5–6. This model may also imply that the magnitude of bidirectional water flow between the open ocean basin and the Oman basin is reduced at this time.

Fike and Grotzinger (2008) argued for an enhanced pyrite sink during the Ara anomaly (~15‰ shift), preserved in the $\delta^{34}S$ record of carbonate-associated sulfate in the deep basinal facies. Fike and Grotzinger (2010) further argued for partial basin restriction associated with the transition from carbonate deposition to gypsum/anhydrite deposition within the SOSB interior. The evolution of $\Delta^{33}S$–$\delta^{34}S$ suggests a possible scenario for the Ara anomaly that is solely due to strongly positive $\delta^{34}S$ of influx sulfur to the oceans without associated enhanced pyrite burial (Fig. 4), and this

[1] The parameter of $f_{py}$ values is the proportion of influx sulfur to the oceans that is buried as pyrite–sulfur at steady states. $f_{py}$ can be evaluated on the basis of pyrite–CAS pairs of $\delta^{34}S$ data, and can be solved as: $f_{py} = \frac{\delta^{34}S_{SW} - \delta^{34}S_{IN}}{\delta^{34}S_{SW} - \delta^{34}S_{PY}}$, where $\delta^{34}S_{IN}$ is the isotopic composition of influx sulfur to the oceans. $f_{py}$ can be also estimated on the basis of CAS $\delta^{34}S$–$\Delta^{33}S$ in the sulfur cycle model that is evaluated by experimental data, and can be solved in the grouped equations (4) (refer to line 131 in the Supplementary materials).

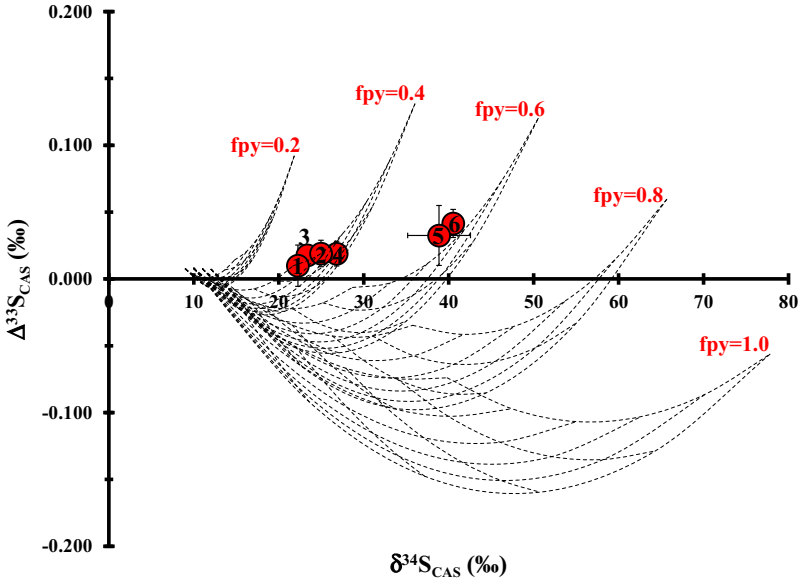


Fig. 3. Plot showing fields of allowed solutions to the global steady state sulfur cycle model with a subset of calculated nets for the sulfur isotopic compositions of oceanic sulfate. For the individual network, the configuration is constrained by three parameters, including the fraction of pyrite burial ($f_{py}$), fraction of sulfate exchange ($f_{ex}$) between seawater and pore water, and fraction of sulfide oxidation ($f_{reox}$). The localities of these networks in the $\delta^{34}S$–$\Delta^{33}S$ space are primarily controlled by the fraction of pyrite burial ($f_{py}$) as the five individual nets presented here. Inside the individual net, the lines are controlled by factors of $f_{ex}$ and $f_{reox}$. The estimates of pyrite fraction burial ($f_{py}$) are slightly dependent on the sulfur isotopic composition of influx sulfur to oceans, but the collective estimates for stages 1–4 are 0.3–0.4, and 0.5–0.6 for stages 5 and 6 with the assumption that the sulfur isotopes of CAS are representative of those of oceanic sulfate in open oceans and may change considerably if basin restriction occurs. In this calculation, the values of input $\delta^{34}S$ and $\Delta^{33}S$ are set to be 10‰ and 0.008‰, respectively (Wu et al., 2010). The red dots represent the averages of oceanic sulfate for the binned strata in Table 1. More details in text. (For interpretation of the references to color in this figure legend, the reader is referred to the web version of this article.)

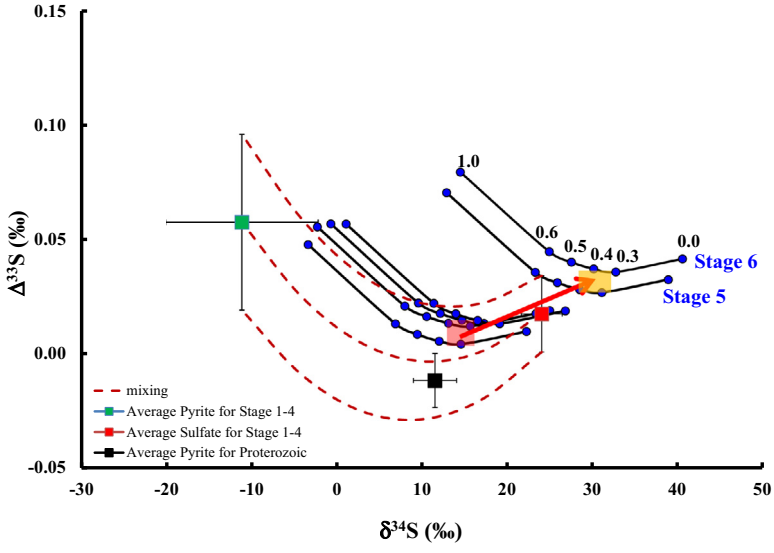


Fig. 4. Plot showing the estimates of $\delta^{34}S$ and $\Delta^{33}S$ of influx sulfur to the oceans during the latest Neoproterozoic and early Cambrian Periods based on the estimate for global sulfur isotope fractionation (25 ± 5‰, Wu et al., 2010) at this time. The individual black lines are estimates for different stages within the Huqf Supergroup with different fractions of pyrite burial between 0 and 1 represented by the points within each line. The red and green squares are averages for $\delta^{34}S$ and $\Delta^{33}S$ at the time for stages 1–4 (this study), and the error bars are the standard deviation of averages to show the spread and evolution of sulfur isotopes of oceanic sulfate and pyrite. The black square is the average for paleo-Proterozoic pyrite–sulfur (Johnston et al., 2006). The solid red line illustrates the evolutionary trend of the sulfur isotopes of input sulfate to the oceans at this time. The red shadow area represents the compositions of influx sulfur for stages 2–4, and the yellow shadow area represents the compositions of influx sulfur for stages 5 and 6. (For interpretation of the references to color in this figure legend, the reader is referred to the web version of this article.)

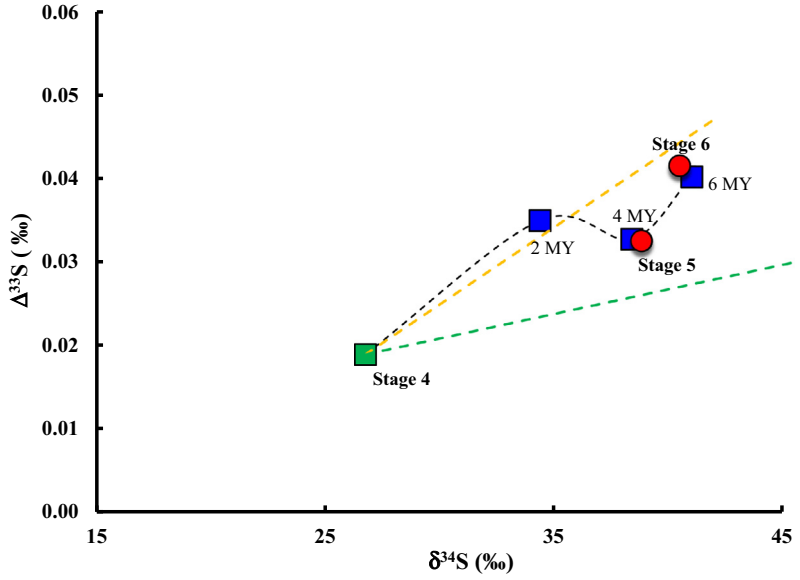


Fig. 5. Simulation results for oceanic sulfate in response to enhanced sulfur influx to the oceans due to rapid recycling of newly formed evaporite minerals. The time interval of 2 Myr is set by the age constraints in the composite strata of the Oman basin (minimum and conservative age constraint for transition between difference oceanic sulfate states). The red dots represent the averages of oceanic sulfate for the binned strata in Table 1. The black dashed line is the isotopic trajectory of the simulation, and the green square is the initial conditions which is set as same as those for stage 4. The blue squares are the projection of this simulation. The yellow and green dashed lines are the trajectories of Rayleigh distillation-like model of sulfur cycling associated with $^{34}\alpha = 0.975$ and $^{34}\alpha = 0.985$, respectively. Detailed descriptions of the simulation are seen in the Supplementary materials. (For interpretation of the references to color in this figure legend, the reader is referred to the web version of this article.)

model carries implications that the sulfur source to the Oman basin is from seawater sulfate from the open oceans, which is different from the sulfur influx to the global oceans at this time that is derived from weathered pyrite, evaporate minerals and volcanic/hydrothermal sulfur.

*4.4.2. Model 2: Enhanced flux from young evaporites*

The composition of sulfate influx determined for stages 1–4 falls within a range of values for $\delta^{34}S$ and $\Delta^{33}S$ that can be explained by a reasonable combination of typical sulfate sources (hydrothermal sources, pyrite oxidation, and weathering of evaporites), but the composition of sulfate influx for stages 5–6 has higher positive $\delta^{34}S$ and $\Delta^{33}S$.

In this second model, we explore the possibility that the $\delta^{34}S$–$\Delta^{33}S$ dynamics for influx sulfate arises as a consequence of rapid cycling of younger evaporite deposits without the usual contributions from weathering of pyrite (Halevy et al., 2012; Wortmann and Adina Paytan, 2012). The effect on $\Delta^{33}S$ due to dissolution of evaporite minerals is explored and simulation results are presented in Fig. 5. The calculation is initialized with present-day estimates of the pyrite sinks, which gives a short residence time compared to that typically quoted for today (10–20 m.y., Claypool et al., 1980; Walker, 1986), and results in a relatively rapid increase of $\delta^{34}S$ and $\Delta^{33}S$ (within a few million years).

The second model also predicts a significant increase in oceanic sulfate concentrations (by an order of magnitude) reaching a value which is comparable to those estimates made on the basis of $[SO_4]/[Cl]$ by Lowenstein et al. (2003) from Ara Group evaporites. This model also carries the implication that dramatic rises in calcium concentrations in the oceans could impact carbonate precipitation at this time. Such implications could possibly be assessed with work on calcium isotopes in the future. If the kinetics of the sinks are not first order, the change in sulfate concentration would be different (lower or higher), but the final steady state condition would still be replicated.

### 4.5. Evaluating the role of oxidative sulfur cycling

Fig. 6 provides a way to evaluate the sulfur cycling between basin sulfate and sedimentary sulfide. This approach examines the relationship of the $\Delta^{33}S$ of sulfate and sulfide and the $\delta^{34}S$ of sulfate and sulfide. Points on this figure represent the fractionations observed for each of the intervals and suggest the sulfur cycle in the Oman basin evolved from a closed to more open sedimentary system (from stage 1 to stage 2 and stage 3) when sulfate exchange between seawater and pore water increased. This could be consistent with the sulfur cycle recovering following the termination of Marinoan glaciation (~635 Ma) when the seawater sulfate in the Proterozoic oceans is thought to be completely drawdown (Hurtgen et al., 2006). It also indicates that a greater proportion of sulfide processed via an oxidation pathway is involved in cycling of sulfur for stage 4, and a smaller role of sulfide oxidation for stages 5 and 6. Progressive oxidation via sulfur disproportionation may be inferred on the basis of the record of sulfur isotope fractionation ($\Delta^{34}S_{CAS\text{-}PY}$, Panel D in Fig. 1, Fike et al., 2006).

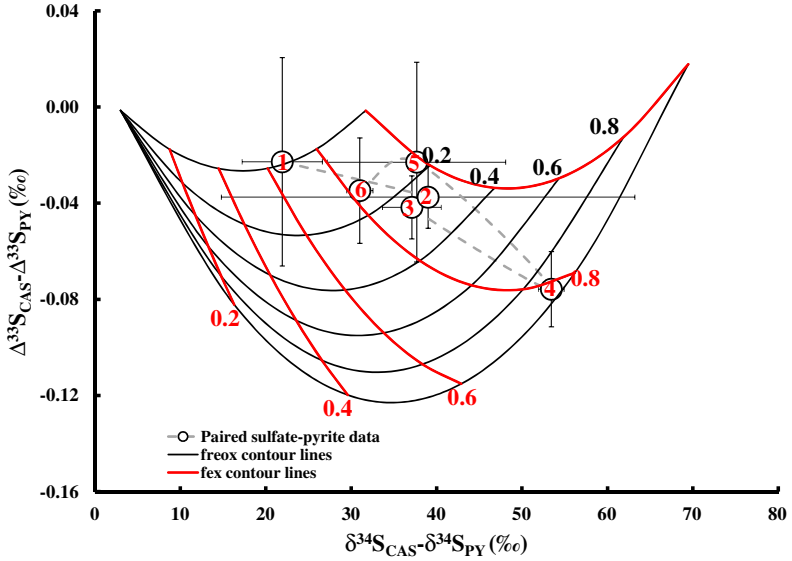


Fig. 6. Plot showing the field of solutions to the sulfur cycle model used in Fig. 3 for paired sulfate–pyrite. The red lines represent the contour for constant $f_{ex}$ but various $f_{reox}$, and the black lines are contour for constant $f_{reox}$ but various $f_{ex}$. The white open dots are data for paired sulfate–pyrite for the binned strata in the Oman basin. The plot is also independent of sulfur isotopic compositions of influx sulfur to the oceans. The vertical and horizontal bars represent uncertainties associated with the calculation. Model specifics are discussed in the Supplementary materials. (For interpretation of the references to color in this figure legend, the reader is referred to the web version of this article.)

There are other interpretations for the $\Delta^{34}S_{CAS\text{-}PY}$. For instance, it may reflect isotope fractionation by only microbial sulfate reduction if the fractionations are very large and the mass dependence of these fractionations approaches the equilibrium limits (see Wortmann et al., 2001; Rudnicki et al., 2001; Brunner and Bernasconi, 2005; Canfield et al., 2010; Sim et al., 2011). To resolve this issue, the relationship between $\Delta^{34}S_{CAS\text{-}PY}$–$\Delta^{33}S_{CAS\text{-}PY}$ can be used to provide independent evidence for sulfide reoxidation (Fig. 6). The oxidation processes that may be important include pathways of forming sulfur intermediates and disproportionative biological and abiological pathways of forming sulfate.

Several inferences can be made from the sulfur cycle models (Figs. 3–5) about the evolution of the isotopic composition of oceanic sulfate. Given the age constraints that exist (Bowring et al., 2007), the observation of a transition from one stable composition to another stable composition over a time scale of less than a few million years, implies comparable residence time ($\sim 10^6$ year) of seawater sulfate. Both models, as well as the evidence for mostly low oxidative cycling (except stage 4, Fig. 6) imply a short residence time of seawater sulfate. Similar suggestions of a short residence time for Neoproterozoic oceanic sulfate have been made by Ries et al. (2009).

We suggest that this short residence time is related to the absence of reoxidation associated with bioturbation (c.f., Canfield and Farquhar, 2009). The residence time of sulfate depends on the total sulfur sink from the oceans ($\varphi_{py} + \varphi_{evap}$). The flux of pyrite burial ($\varphi_{py}$) is approximated by the difference between the flux of sulfate reduced by bacteria and the flux of sulfide reoxidized ($\varphi_{SRB} - \varphi_{reox}$). While reoxidation of sulfide must have occurred prior to reoxidation associated with bioturbation, Canfield and Farquhar (2009) have argued that bioturbation will generate a significant enhancement in reoxidation rates, resulting in higher sulfate concentrations and longer residence times. The transition from one steady state to another in the Ediacaran implies a short residence time. It might be predicted that once sulfide reoxidation played a prominent role, that the residence time would lengthen sufficiently to yield looped trajectories for $\delta^{34}S$ and $\Delta^{33}S$ of oceanic sulfate.

## 5. SUMMARY

Multiple sulfur isotopes ($\Delta^{33}S$ and $\delta^{34}S$) of carbonate-associated sulfate and sedimentary pyrite from the Huqf Supergroup in Oman are presented in this study. Oceanic sulfur cycle models designed to evaluate the relationships between $\Delta^{33}S$ and $\delta^{34}S$ records provide a way to test hypotheses and inferences made previously on the basis of $\delta^{34}S$ alone, and give additional insight into evolution of the sulfur cycle at this time (e.g., estimates of sulfur isotopes of influx sulfur to the oceans and the role of sulfide reoxidation in the sulfur cycle).

The modeled results suggest the sulfur cycle at the time sediments of middle strata of Huqf Supergroup (stages 2–4) were deposited mirrored the global cycle of that time. The stability of the sulfur isotopic records (Fig. 1) and the average $\Delta^{33}S$ and $\delta^{34}S$ are consistent with the assertion that these records track global oceanic sulfate, and the global average composition of sedimentary pyrite that was fed by a riverine sulfate influx with a stable sulfur isotope composition having significantly positive $\Delta^{33}S$ and $\delta^{34}S$ for stages 2–4.

The $\Delta^{33}S$ and $\delta^{34}S$ data from the upper parts of Huqf Supergroup suggest that sulfur flux to the Oman basin became more $^{34}S$-enriched and more positive $\Delta^{33}S$ during the latest Neoproterozoic. The more positive $\Delta^{33}S$ of source/influx sulfate to the Oman basin at this time can be reconciled with a 60-fold enhancement of evaporite weathering sources accompanied by a short (1–2 m.y.) response time for oceanic sulfate. It is also possible to explain it with a very different (basin-scale) model that attributes the change in composition of the influx sulfate resulting from partial restriction of the Oman basin accompanied by a significant local pyrite sink. This latter model is not supported by the observation of abundant evaporites in other parts of the Oman basin and sulfate levels by fluid inclusion analysis (Horita et al., 2002; Lowenstein et al., 2003) or by the $\delta^{34}S$ agreement between CAS and anhydrite (Fike and Grotzinger, 2008, 2010). Geological and geochemical data from the Oman basin and $\delta^{34}S$ excursions that occurred in basins in other parts of the world at this time appear to support the hypothesis of enhanced evaporite weathering rather than the interpretation of partial closing of the Oman basin, but the magnitude and timing of these excursions in the late Ediacaran basins need to be further reconciled to reinforce this conclusion.

## ACKNOWLEDGMENTS

This study was supported by an NSF – United States Grant (EAR 0918382). We thank Petroleum Development Oman for access to samples. Helpful comments by Alan Jay Kaufman greatly improved this text.

## APPENDIX A. SUPPLEMENTARY DATA

Supplementary data associated with this article can be found, in the online version, at http://dx.doi.org/10.1016/j.gca.2015.05.031.

## REFERENCES

Amthor J. E., Grotzinger J. P., Schroder S., Bowring S. A., Ramezani J., Martin M. W. and Matter A. (2003) Extinction of Cloudina and Namacalathus at the Precambrian–Cambrian boundary in Oman. *Geology* **31**, 431–434.

Bartley J. K. and Kah L. C. (2004) Marine carbon reservoir, Corg-Ccarb coupling, and the evolution of the Proterozoic carbon cycle. *Geology* **32**(2), 129–132.

Bowring S. A., Myrow P. M., Landing E. and Ramezani J. (2002) Geochronological constraints on terminal Neoproterozoic events and the rise of Metazoans. *Astrobiology* **2**, 112.

Bowring S. A., Grotzinger J. P., Condon D. J., Ramezani J. and Newall M. (2007) Geochronologic constraints on the chronostratigraphic framework of the Neoproterozoic Huqf Supergroup, Sultanate of Oman. *Am. J. Sci.* **307**, 1097–1145.

Brennan S. T., Lowenstein T. K. and Horita J. (2004) Seawater chemistry and the advent of biocalcification. *Geology* **32**(6), 473–476.

Brunner B. and Bernasconi S. M. (2005) A revised isotope fractionation model for dissimilatory sulfate reduction in sulfate reducing bacteria. *Geochim. Cosmochim. Acta* **69**(20), 4759–4771.

Burns S. J. and Matter A. (1993) Carbon isotopic record of the latest Proterozoic from Oman. *Eclog. Geol. Helv.* **86**, 595–607.

Calver C. R. (2000) Isotope stratigraphy of the Ediacaran (Neoproterozoic III) of the Adelaide Rift Complex, Australia, and the overprint of water column stratification. *Precambr. Res.* **100**, 121–150.

Canfield D. E. (2001) Biogeochemistry of sulfur isotopes. *Rev. Mineral. Geochem.* **43**, 607–636.

Canfield D. E. (2004) The evolution of the Earth surface sulfur reservoir. *Am. J. Sci.* **304**, 839–861.

Canfield D. E. and Farquhar J. (2009) Animal evolution, bioturbation, and the sulfate concentration of the oceans. *Proc. Natl. Acad. Sci. U.S.A.* **106**(20), 8123–8127.

Canfield D. E., Poulton S. W. and Narbonne G. M. (2007) Late Neoproterozoic deep ocean oxygenation and the rise of animal life. *Science* **315**, 92–95.

Canfield D. E., Poulton S. W., Knoll A. H., Narbonne G. M., Ross G., Goldberg T. and Strauss H. (2008) Ferruginous conditions dominated later Neoproterozoic deep-water chemistry. *Science* **321**, 949–952.

Canfield D. E., Farquhar J. and Zerkle A. L. (2010) High isotope fractionations during sulfate reduction in a low-sulfate euxinic ocean analog. *Geology* **38**(5), 415–418.

Claypool G. E., Holser W. T., Kaplan I. R., Sakai H. and Zak I. (1980) The age curves of sulfur and oxygen isotopes in marine sulfate and their mutual interpretation. *Chem. Geol.* **28**, 199–260.

Crowe S. A., Paris G., Katsev S., Jones C., Kim S.-T., Zerkle A. L., Nomosatryo S., Fowle D. A., Adkins J. F., Sessions A. L., Farquhar J. and Canfield D. E. (2014) Sulfate was a trace constituent of Archean seawater. *Science* **346**, 735–739.

Dahl T. W., Hammarlund E. U., Anbar A. D., Bond D. P. G., Gill B. C., Gordon G. W., Knoll A. H., Nielsen A. T., Schovsbo N. H. and Canfield D. E. (2010) Devonian rise in atmospheric oxygen correlated to the radiations of terrestrial plants and large predatory fish. *Proc. Natl. Acad. Sci.* **107**, 17911–17915.

Detmers J., Brüchert V., Habicht K. S. and Kuever J. (2001) Diversity of sulfur isotope fractionations by sulfate-reducing prokaryotes. *Appl. Environ. Microbiol.* **67**, 888–894.

Fike D.A. (2007) Carbon and sulfur isotopic constraints on Ediacaran biogeochemical processes, Huqf Supergroup, Sultanate of Oman. Ph.D. Thesis, Massachusetts Institute of Technology.

Fike D. A. and Grotzinger J. P. (2008) A paired sulfate-pyrite $\delta^{34}S$ approach to understanding the evolution of the Ediacaran–Cambrian sulfur cycle. *Geochim. Cosmochim. Acta* **72**(11), 2636–2648.

Fike D. A. and Grotzinger J. P. (2010) A $\delta^{34}SSO4$ approach to reconstructing biogenic pyrite burial in carbonate-evaporite basins: an example from the Ara Group, Sultanate of Oman. *Geology* **38**(4), 371–374.

Fike D. A., Grotzinger J. P., Pratt L. M. and Summons R. E. (2006) Oxidation of the Ediacaran Ocean. *Nature* **444**, 744–747.

Gomes M. L. and Hurtgen M. T. (2013) Sulfur isotope systematics of a euxinic, low-sulfate lake: evaluating the importance of the reservoir effect in modern and ancient oceans. *Geology* **41**(6), 663–666.

Grotzinger J. P., Bowring S. A., Saylor B. Z. and Kaufman A. J. (1995) Biostratigraphic and geochronological constraints on early animal evolution. *Science* **270**, 598–604.

Grotzinger J. P., Al-Siyabi A. H., Al-Hashimi R. A. and Cozzi A. (2002) New model for tectonic evolution of Neoproterozoic-Cambrian Huqf Supergroup basins, Oman. *GeoArabia* **7**, 241.

Grotzinger J. P., Fike D. A. and Fischer W. W. (2011) Enigmatic origin of the largest-known carbon isotope excursion in Earth's history. *Nat. Geosci.* **4**, 285–292.

Habicht K. S., Gade M., Thamdrup B., Berg P. and Canfield D. E. (2002) Calibration of sulfate levels in the Archean Ocean. *Science* **298**, 2372–2374.

Halevy I., Peters S. E. and Fisher W. W. (2012) Sulfate burial constraints on the phanerozoic sulfur cycle. *Science* **337**, 331–334.

Horita J., Zimmermann H. and Holland H. D. (2002) Chemical evolution of seawater during the Phanerozoic: implications from the record of marine evaporites. *Geochim. Cosmochim. Acta.* **66**, 3733–3756.

Hurtgen M. T., Halverson G. P., Arthur M. A. and Hoffman P. F. (2006) Sulfur cycling in the aftermath of a 635-Ma snowball glaciation: evidence for a syn-glacial sulfidic deep ocean. *Earth Planet. Sci. Lett.* **245**(3–4), 551–570.

Johnston D. T., Wing B. A., Farquhar J., Kaufman A. J., Strauss H., Lyons T. W., Kah L. C. and Canfield D. E. (2005) Active microbial sulfur disproportionation in the Mesoproterozoic. *Science* **310**, 1477–1479.

Johnston D. T., Poulton S. W., Fralick P. W., Wing B. A., Canfield D. E. and Farquhar J. (2006) Evolution of the oceanic sulfur cycle at the end of the Paleoproterozoic. *Geochim. Cosmochim. Acta* **70**, 5723–5739.

Johnston D. T., Farquhar J. and Canfield D. E. (2007) Sulfur isotope insights into microbial sulfate reduction: when microbes meet models. *Geochim. Cosmochim. Acta* **71**, 3929–3947.

Johnston D. T., Farquhar J., Habicht K. S. and Canfield D. E. (2008a) Sulphur isotopes and the search for life: strategies for identifying sulphur metabolisms in the rock record and beyond. *Geobiology* **6**, 425–435.

Johnston D. T., Farquhar J., Summons R., Shen Y., Kaufman A. J., Masterson A. L. and Canfield D. E. (2008b) Late Paleo-Mesoproterozoic sulfur isotope biogeochemistry: insight from the McArthur Basin. *Geochim. Cosmochim. Acta* **72**, 4278–4290.

Johnston D. T., Poulton S. W., Goldberg T., Sergeev V. N., Podkovyrov V., Vorob'eva N., Bekker A. and Knoll A. H. (2012) Late Ediacaran redox stability and metazoan evolution. *Earth Planet. Sci. Lett.* **335–336**, 25–35.

Johnston D. T., Poulton S. W., Tosca N. J., O'Brien T., Halverson G. P., Schrag D. P. and Macdonald F. A. (2013) Searching for an oxygenation event in the fossiliferous Ediacaran of northwest Canada. *Chem. Geol.* **362**(2013), 273–286.

Kah L. C., Lyons T. W. and Frank T. D. (2004) Low marine sulphate and protracted oxygenation of the proterozoic biosphere. *Nature* **431**, 834–838.

Kaufman A. J., Corsetti F. A. and Varni M. A. (2007) The effect of rising atmospheric oxygen on carbon and sulfur isotope anomalies in the Neoproterozoic Johnnie Formation, Death Valley, USA. *Chem. Geol.* **237**, 47–63.

Laflamme M., Darroch S., Tweedt S. M., Peterson K. J. and Erwin D. H. (2013) The end of the Ediacara biota: extinction, biotic replacement, or Cheshire Cat? *Gondwana Res.* **23**(2), 558–573.

Le Guerroue E., Allen P. A. and Cozzi A. (2006) Chemostratigraphic and sedimentological framework of the largest negative carbon isotopic excursion in Earth history: the Neoproterozoic Shuram Formation (Nafun Group, Oman). *Precambr. Res.* **146**, 68–92.

Leavitt W. D., Halevy I., Bradley A. S. and Johnston D. T. (2013) Influence of sulfate reduction rates on the Phanerozoic sulfur isotope record. *Proc. Natl. Acad. Sci. U.S.A.*. http://dx.doi.org/10.1073/pnas.1218874110.

Li C., Love G. D., Lyons T. W., Fike D. A., Sessions A. L. and Chu X. (2010a) A stratified redox model for the Ediacaran Ocean. *Science* **328**, 80–83.

Li X. N., Gilhooly W. P., Zerkle A. L., Lyons T. W., Farquhar J., Werne J. P., Varela R. and Scranton M. I. (2010b) Stable sulfur isotopes in the water column of the Cariaco Basin. *Geochim. Cosmochim. Acta* **74**(23), 6764–6778.

Li D., Ling H.-F., Shields-Zhou G. A., Chen X., Cremonese L., Och L., Thirlwall M. and Manning C. J. (2013) Carbon and strontium isotope evolution of seawater across the Ediacaran–Cambrian transition: evidence from the Xiaotan section, NE Yunnan, South China. *Precambr. Res.* **225**, 128–147.

Lowenstein T. K., Hardie L. A., Timofeff M. N. and Demicco R. V. (2003) Secular variation in seawater chemistry and the origin of calcium chloride basinal brines. *Geology* **31**, 857–860.

Loyd S. J., Marenco P. J., Hagadorn J. W., Lyons T. W., Kaufman A. J., Sour-Tovar F. and Corsetti F. A. (2012) Sustained low marine sulfate concentrations from the Neoproterozoic to the Cambrian: insights from carbonates of northwestern Mexico and eastern California. *Earth Planet. Sci. Lett.* **339–340**, 79–94.

Loyd S. J., Marenco P. J., Hagadorn J. W., Lyons T. W., Kaufman A. J., Sour-Tovar F. and Corsetti F. A. (2013) Local $\delta^{34}S$ variability in ~580 Ma carbonates of northwestern Mexico and the Neoproterozoic marine sulfate reservoir. *Precambr. Res.* **224**, 551–569.

Maloof A. C., Porter S. M., Moore J. L., Dudas F. O., Bowring S. A., Higgins J. A., Fike D. A. and Eddy M. P. (2010) The earliest Cambrian record of animals and ocean geochemical change. *Geol. Soc. Am. Bull.* **122**(11–12), 1731–1774.

Mattes B. W. and Conway-Morris S. (1990) Carbonate/evaporite deposition in the Late Precambrian-Early Cambrian Ara Formation of southern Oman. In *The Geology and Tectonics of the Oman Region* (eds. A. H. F. Robertson, M. P. Searle and A. C. Ries). Geological Society, London.

McCarron G. (2000) The sedimentology and chemostratigraphy of the Nafun Group, Huqf Supergroup, Oman. Ph. D. Thesis, Oxford University, p. 175.

McFadden K. A., Huang J., Chu X., Jiang G., Kaufman A. J., Zhou C., Yuan X. and Xiao S. (2008) Pulsed oxidation and biological evolution in the Ediacaran Doushantuo Formation. *Proc. Natl. Acad. Sci. U.S.A.* **105**, 3197–3202.

Narbonne G. M. (2005) The Ediacara biota: Neoproterozoic origin of animals and their ecosystems. *Annu. Rev. Earth Planet. Sci.* **33**, 421–442.

Ono S., Wing B., Johnston D., Farquhar J. and Rumble D. (2006) Mass-dependent fractionation of quadruple stable sulfur isotope system as a new tracer of sulfur biogeochemical cycles. *Geochim. Cosmochim. Acta* **70**(9), 2238–2252.

Raab M. and Spiro B. (1991) Sulfur isotopic variations during seawater evaporation with fractional crystallization. *Chem. Geol. Isot. Geosci. Sect.* **86**, 323–333.

Rees C. E. (1978) Sulphur isotope measurements using $SO_2$ and $SF_6$. *Geochim. Cosmochim. Acta* **42**, 383–389.

Ries J. B., Fike D. A., Pratt L. M., Lyons T. W. and Grotzinger J. P. (2009) Superheavy pyrite ($\delta^{34}S_{pyr} > \delta^{34}S_{CAS}$) in the terminal Proterozoic Nama Group, southern Namibia: a consequence of low seawater sulfate at the dawn of animal life. *Geology* **37**, 743–746.

Rudnicki M. D., Elderfield H. and Spiro B. (2001) Fractionation of sulfur isotopes during bacterial sulfate reduction in deep ocean sediments at elevated temperatures. *Geochim. Cosmochim. Acta* **65**(5), 777–789.

Schröder S., Schreiber B. C., Amthor J. E. and Matter A. (2003) A depositional model for the terminal Neoproterozoic–Early Cambrian Ara Group evaporites in south Oman. *Sedimentology* **50**, 879–898.

Schröder S., Schreiber B. C., Amthor J. E. and Matter A. (2004) Stratigraphy and environmental conditions of the terminal Neoproterozoic–Cambrian period in Oman: evidence from sulphur isotopes. *J. Geol. Soc.* **161**, 489–499.

Schröder S., Grotzinger J. P., Amthor J. E. and Matter A. (2005) Carbonate deposition and hydrocarbon reservoir development at the Precambrian–Cambrian boundary: the Ara Group in South Oman. *Sediment. Geol.* **180**, 1–28.

Sim M. S., Bosak T. and Ono S. (2011) Large sulfur isotope fractionation does not require disproportionation. *Science* **333**, 74–77.

Walker J. C. G. (1986) Global geochemical cycles of carbon, sulfur and oxygen. *Mar. Geol.* **70**(1–2), 159–174.

Wing B. A. and Halevy I. (2014) Intracellular metabolite levels shape sulfur isotope fractionation during microbial sulfate reduction. *Proc. Natl. Acad. Sci. USA* **111**(51), 18116–18125.

Wortmann U. G. and Adina Paytan A. (2012) Rapid variability of seawater chemistry over the past 130 million years. *Science* **337**, 334–336.

Wortmann U. G. and Chernyavsky B. M. (2007) Effect of evaporite deposition on Early Cretaceous carbon and sulphur cycling. *Nature* **446**, 654–656.

Wortmann U. G., Bernasconi S. M. and Bottcher M. E. (2001) Hypersulfidic deep biosphere indicates extreme sulfur isotope fractionation during single-step microbial sulfate reduction. *Geology* **29**(7), 647–650.

Wotte T., Shields-Zhou G. A. and Strauss H. (2012) Carbonate-associated sulfate: experimental comparisons of common extraction methods and recommendations toward a standard analytical protocol. *Chem. Geol.* **326–327**, 132–144.

Wu N. P., Farquhar J., Strauss H., Kim S. T. and Canfield D. E. (2010) Evaluating the S-isotope fractionation associated with Phanerozoic pyrite burial. *Geochim. Cosmochim. Acta* **74**(7), 2053–2071.

Xiao S., McFadden K. A., Peek S., Kaufman A. J., Zhou C., Jiang G. and Hu J. (2012) Integrated chemostratigraphy of the Doushantuo Formation at the northern Xiaofenghe section (Yangtze Gorges, South China) and its implication for Ediacaran stratigraphic correlation and ocean redox models. *Precambr. Res.* **192–195**, 125–141.

Zerkle A. L., Farquhar J., Johnston D. T., Cox R. P. and Canfield D. E. (2009) Fractionation of multiple sulfur isotopes during phototrophic oxidation of sulfide and elemental sulfur by a green sulfur bacterium. *Geochim. Cosmochim. Acta* **73**, 291–306.

*Associate editor:* Timothy Lyons